Molecular scattering wave functions for Auger decay rates: The Auger spectrum of hydrogen fluoride

K. Zähringer, H.-D. Meyer, and L. S. Cederbaum
Theoretische Chemie, Physikalisch Chemisches Institut, Universität Heidelberg, Im Neuenheimer Feld 253, D-6900 Heidelberg, Federal Republic of Germany
(Received 1 April 1991)

A numerical method for calculating Auger rates is proposed. The continuum wave of the ejected Auger electron is computed by numerical propagation (close-coupling method) and thus accounts for the nonspherical interaction with the molecule. The method is tested by computing the Auger spectrum of hydrogen fluoride. Here initial cationic and final dicationic states are treated on the self-consistent-field level.

PACS number(s): 33.80.Eh, 32.80.Hd, 34.80.Kw

I. INTRODUCTION

Auger electron spectroscopy has become a valuable probe of the electronic structure of molecules. A careful theoretical analysis of the Auger spectrum requires not only the computation of the Auger energies but of the Auger intensities as well.

The calculation of the Auger energies can be performed by employing standard [1] and less standard [2,3] quantum-chemistry methods. The calculation of the Auger rates, on the other hand, requires the knowledge of the continuum wave function of the ejected Auger electron. Such a molecular continuum wave function can be evaluated by adopting methods developed for the study of electron-molecule scattering [4–6]. We note in passing that quite similar problems arise when studying the (molecular) photoionization process [5,7].

In order to circumvent the somewhat elaborate calculation of the continuum wave there have been attempts to approximate the molecular continuum wave by a plane wave [8,9], a Coulomb wave [10], or an atomic continuum wave [11–13]. The latter approach is a useful approximation in particular for "atomic-like" molecules as, e.g., HF, H_2O, CH_4, etc. The other two approximations, however, yield results that can be severely wrong. We emphasize that only a molecular continuum wave allows for an evaluation of the angular distribution of the Auger electrons.

Our approach to compute the molecular continuum wave consists of a single-center expansion of the interaction potential and the wave function. The resulting close-coupling equations for the wave function are integrated numerically. The interaction potential determining the continuum wave was chosen to be the static-exchange potential [4], i.e., the electrostatic and the exchange interaction of the continuum electron with the "frozen" charge distribution of the final dictation. The wave function that determines the charge distribution may be fully correlated and is not required to be a self-consistent-field (SCF) state. We have replaced the (nonlocal) exchange interaction by a local model potential [4,14]. A local model exchange should be sufficient because of the high kinetic energy of the ejected Auger electron. We have found in this work that the total effect of the exchange potential is relatively small. This clearly justifies our use of an approximate local exchange potential.

One of the first attempts to generate a molecular continuum wave for computing Auger rates is the contribution of Higashi, Hiroike, and Nakojima [15]. They ignored the exchange completely and approximately solved the coupled equations in two steps by introducing a decoupling scheme. Larkins and Richards [16], on the other hand, avoided the single-center expansion and computed the continuum wave of linear molecules by integration over a (r,θ) grid. The exact exchange was included. Their work concentrated on the study of Li_2.

In contrast to the numerical integration methods, L^2-basis-set methods have been tried as well. Colle and Simonucci [17] determined the continuum wave by solving the Lippman-Schwinger equation within a Gaussian basis set. Carravetta and Ågren [18], on the other hand, have tried to avoid the explicit construction of a continuum wave by adopting the Stieltjes imaging method [19], which has been amply applied [19] before to the evaluation of photoionization cross sections. Stieltjes imaging cannot be used to compute the angular distribution of the Auger electrons.

It is the purpose of the present paper to introduce and describe the proposed method for computing molecular Auger rates. As an example, we also present a calculation on the Auger spectrum of the HF molecule. The paper is organized as follows. In Sec. II we discuss the evaluation of Auger rates using a nonrelativistic first-order treatment (Wentzel's approach [20]). In Sec. III we briefly discuss our method for determining the continuum wave and matrix elements thereof. In Sec. IV we discuss the Auger spectrum of HF and in particular discuss the validity of different approximations. In Sec. V we finally conclude our findings.

II. AUGER RATES

We consider the Auger effect as a two-step process in which the Auger decay can be treated separately from the initial ionization. The ionization step is of no further interest. The decay process can be conveniently evaluated by employing Fermi's golden rule. As is usual in the context of the golden rule it is required to split the Hamiltonian into two parts, H_0+V. The interaction V accomplishes the decay in question. H_0 is derived from the full H by deleting all terms that lead to a decay. The golden-rule expression for the Auger rate reads

$$\Gamma_{f,i}\equiv 2\pi|\langle\Psi_f^{(N-1)}|V|\Psi_i^{(N-1)}\rangle|^2 . \tag{2.1a}$$

Here $|\Psi_i^{(N-1)}\rangle$ denotes the initial core-ionized state and the subscript $N-1$ denotes the number of electrons where N is the number of electrons of the neutral molecule. The subscript i (f) stands for initial (final). Both the initial and final states are eigenfunctions of H_0 with total energy E. Because $V=H-H_0$ we may rewrite the above equation to give the well-known Wentzel expression,

$$\Gamma_{f,i}=2\pi|\langle\Psi_f^{(N-1)}|H-E|\Psi_i^{(N-1)}\rangle|^2 . \tag{2.1b}$$

The very use of the golden rule implies the separability of the core and valence electrons in H_0 and hence in the wave functions. The interaction between the core and valence electrons gives rise to the decay and is included in V. In the following we evaluate the expression (2.1b) for the Auger decay rate. We would like to mention that this formula has been previously evaluated [21] without requiring the wave functions to be eigenfunctions of H_0. The final expression obtained is somewhat different from ours.

The final state $|\Psi_f^{(N-1)}\rangle$ is a continuum wave function that is assumed to be energy normalized. Since the energy of the Auger electron is high, it is quite reasonable to assume that this electron does not correlate with the other electrons of the dictation. Hence, we approximate $|\Psi_f^{(N-1)}\rangle$ by the product

$$|\Psi_f^{(N-1)}\rangle=\mathcal{A}(\psi_\varepsilon^-|\Psi_f^{(N-2)}\rangle) , \tag{2.2}$$

where $\mathcal{A}$ denotes the anitsymmetrizer and ψ_ε^- denotes the one particle continuum wavefunction of the Auger electron. The minus sign indicates the incoming asymptotic boundary condition and the subscript ε denotes the final kinetic energy of the Auger electron. The symbol $|\Psi_f^{(N-1)}\rangle$ denotes the final dicationic state of the molecule with energy $E_f=\langle\Psi_f^{(N-2)}|H_0|\Psi_f^{(N-2)}\rangle=\langle\Psi_f^{(N-2)}|H|\Psi_f^{(N-2)}\rangle$. Because of energy conservation we have, of course,

$$\varepsilon=E-E_f \tag{2.3}$$

Introducing the creation operator $a_\varepsilon^\dagger$ for the wave function ψ_ε^-

$$a_\varepsilon^\dagger=\int\psi_\varepsilon^-(\mathbf{x})\hat{\Psi}^\dagger(\mathbf{x})d\mathbf{x} , \tag{2.4}$$

where $\hat{\Psi}(\mathbf{x})$ denotes the field operator [22], we can write Eq. (2.2) more compactly as

$$|\Psi_f^{(N-1)}\rangle=a_\varepsilon^\dagger|\Psi_f^{(N-2)}\rangle . \tag{2.5}$$

To satisfy the spin symmetry for both $|\Psi_f^{(N-1)}\rangle$ and $|\Psi_f^{(N-2)}\rangle$ a slightly more complicated form may have to be used. See the Appendix for details. Note that the neglect of correlation between the Auger electron and the electrons of the final dicationic state implies the neglect of final-state-channel coupling; i.e., a single-channel approximation is made. Final-state channel coupling has been investigated by Howat, Aberg, and Goscinski [23] for atoms and recently by Colle and Simonucci [24]. In the latter investigation, L^2 methods are used that allow for treating molecules as well.

The core-valence separability assumes that the core electron does not correlate with the other electrons and that the core orbital is independent of the electronic state of the molecule. For not too light atoms this is an excellent approximation because of the large energy gap between core and valence states. Denoting by $a_{c\alpha}^\dagger$ and $a_{c\beta}^\dagger$ the creation operators of the core orbital of spin α or β, respectively, we write

$$|\Psi_i^{(N-1)}\rangle=a_{c\alpha}^\dagger|\Psi_i^{(N-2)}\rangle , \tag{2.6}$$

$$|\Psi_f^{(N-1)}\rangle=a_\varepsilon^\dagger a_{c\alpha}^\dagger a_{c\beta}^\dagger|\Psi_f^{(N-4)}\rangle \tag{2.7}$$

and further require that

$$a_{c\alpha}|\Psi_i^{(N-2)}\rangle=a_{c\beta}|\Psi_i^{(N-2)}\rangle=0 , \tag{2.8a}$$

$$a_{c\alpha}|\Psi_f^{(N-4)}\rangle=a_{c\beta}|\Psi_f^{(N-4)}\rangle=0 \tag{2.8b}$$

hold, i.e., the wave functions $|\Psi_i^{(N-2)}\rangle$ and $|\Psi_f^{(N-4)}\rangle$ contain no contribution from the core orbitals.

In order to proceed we introduce an orthogonal set of spin orbitals $\{\varphi_i\}$. At the present stage this set is arbitrary but must contain the core orbitals $\varphi_{c\alpha}$ and $\varphi_{c\beta}$. Corresponding to these spin orbitals we introduce the creation and annihilation operators $a_i^\dagger$ and a_i and write the Hamiltonian in its second-quantized form

$$H=\sum_{i,j}T_{ij}a_i^\dagger a_j+\tfrac{1}{2}\sum_{i,j,k,l}V_{i,j,k,l}a_i^\dagger a_j^\dagger a_l a_k . \tag{2.9}$$

Here $T_{i,j}$ denotes the matrix elements of the one-particle part (bare nucleus Hamiltonian) and

$$V_{i,j,k,l}=\int d\mathbf{x}\,d\mathbf{x}'\varphi_i(\mathbf{x})^*\varphi_j(\mathbf{x}')^*|\mathbf{r}-\mathbf{r}'|^{-1}\varphi_k(\mathbf{x})\varphi_l(\mathbf{x}') . \tag{2.10}$$

The symbol $\mathbf{x}$ stands here for a spin-space variable, the spatial part of which is denoted by $\mathbf{r}$. Atomic units are used throughout.

We now can evaluate the Auger rate (2.1). The amplitude

$$A_{f,i}=\langle\Psi_f^{(N-1)}|H-E|\Psi_i^{(N-1)}\rangle$$

takes the appearance

$$A_{f,i}=\langle\Psi_f^{(N-4)}|a_{c\beta}a_{c\alpha}a_\varepsilon Ha_{c\alpha}^\dagger|\Psi_i^{(N-2)}\rangle . \tag{2.11}$$

Using Eq. (2.9) and commuting all creation operators to the left one arrives after a short calculation at

$$A_{f,i}=-\sum_{l,m}(V_{c\beta,\varepsilon,k,l}-\langle\psi_\varepsilon^-|\varphi_{c\alpha}\rangle V_{c\beta,c\alpha,k,l})\times\langle\Psi_f^{(N-4)}|a_k a_l|\Psi_i^{(N-2)}\rangle-\sum_j(T_{c\beta,j}+V_{c\beta,c\alpha,j,c\alpha})\langle\Psi_f^{(N-4)}|a_j a_\varepsilon|\Psi_i^{(N-2)}\rangle+\sum_{j,k,l}V_{c\beta,j,k,l}\langle\Psi_f^{(N-4)}|a_j^\dagger a_k a_l a_\varepsilon|\Psi_i^{(N-2)}\rangle\ . \quad (2.12)$$

Equation (2.12) is the final result for the ansatz (2.6)–(2.8). We note in passing that this equation simplifies considerably when $a_\varepsilon|\Psi_i^{(N-1)}\rangle=0$ holds, i.e., when the continuum orbital ψ_ε^- does not overlap with the occupied orbitals of the *initial* state. In this case (2.12) assumes the simple appearance

$$A_{f,i}=-\sum_{k,l}V_{c\beta,\varepsilon,k,l}\langle\Psi_f^{(N-4)}|a_k a_l|\Psi_i^{(N-2)}\rangle\ . \quad (2.13)$$

However, we emphasize that there is no reason why $a_\varepsilon|\Psi_i^{(N-1)}\rangle=0$ should hold rigorously. The orthogonality of the many-electron scattering states $|\Psi_f^{(N-1)}\rangle$ ensures that the exact scattered wave ψ_ε^- satisfies $a_\varepsilon|\Psi_f^{(N-2)}\rangle=0$. Due to the high energy of the Auger electron one can safely assume that $||a_\varepsilon|\Psi_i^{(N-1)}\rangle||$ is small but its neglect is an approximation. We, therefore, consider the full expression (2.12).

The result (2.12) is for general correlated wave functions $|\Psi_i^{(N-2)}\rangle$ and $|\Psi_f^{(N-4)}\rangle$. From now on we explicitly consider the case where the *initial* state $|\Psi_i^{(N-1)}\rangle$ is given by a single determinant of SCF orbitals. In this case the creation operators $a_j^\dagger$ are chosen to correspond to a set of SCF orbitals of the initial state $|\Psi_i^{(N-1)}\rangle$. Splitting the last term of Eq. (2.12) into a sum over occupied (with respect to $|\Psi_i^{(N-1)}\rangle$) and virtual orbitals we obtain

$$A_{f,i}=-\sum_{k,l}^{\text{occ}}V_{c\beta,\varepsilon_\perp,k,l}\langle\Psi_f^{(N-4)}|a_k a_l|\Psi_i^{(N-2)}\rangle-\sum_j^{\text{occ}}\left[T_{c\beta,j}+\sum_l^{\text{occ}}V_{c\beta,l,[j,l]}\right]\langle\Psi_f^{(N-4)}|a_j a_\varepsilon|\Psi_i^{(N-2)}\rangle+\sum_j^{\text{vir}}\sum_{k,l}^{\text{occ}}V_{c\beta,j,k,l}\langle\Psi_f^{(N-4)}|a_j^\dagger a_k a_l a_\varepsilon|\Psi_i^{(N-2)}\rangle\ , \quad (2.14)$$

where $V_{i,j,[k,l]}\equiv V_{i,j,k,l}-V_{i,j,l,k}$ denotes the antisymmetrized Coulomb matrix element. The symbol

$$V_{c\beta,\varepsilon_\perp,[k,l]}\equiv V_{c\beta,\varepsilon,[k,l]}-\sum_j^{\text{occ}}V_{c\beta,j,[k,l]}\langle\psi_\varepsilon^-|\varphi_j\rangle \quad (2.15)$$

is nothing but the Coulomb matrix element of a continuum wave orthogonalized with respect to the occupied orbitals of the *initial* state $|\Psi_i^{(N-1)}\rangle$. We remind the reader that by a sum over occupied orbitals we denote a sum over those orbitals that are occupied in the initial $|\Psi_i^{(N-1)}\rangle$ state; e.g., $\varphi_{c\alpha}$ is an occupied orbital but $\varphi_{c\beta}$ is not.

The second term of Eq. (2.14) vanishes because of the diagonality of the Fock operator. This is obvious when the orbitals of the unrestricted Hartree-Fock (UHF) procedure are used. Moreover, the second term of Eq. (2.14) still vanishes when adopting the restricted Hartree-Fock (RHF) orbitals. This can be easily proved by recognizing that there is only one singly occupied orbital available. All other (spatial) orbitals of the initial state are either doubly occupied or vacant.

The last term of Eq. (2.14) yields a very small contribution because both $\|a_\varepsilon|\Psi_i^{(N-1)}\rangle\|$ and $\|a_j|\Psi_f^{(N-4)}\rangle\|$ (j virtual) are small. In our calculations presented in Sec. IV we have always neglected this term. For the hydrogen fluoride this neglect is clearly justified. For other molecules, in particular for cases in which $a_j|\Psi_f^{(N-4)}\rangle$ (j virtual) becomes appreciable, one may wish to keep this term. However, we presume that the last term of Eq. (2.14) is negligible in most cases.

We now turn to the first term of Eq. (2.14). To evaluate it one has to compute the Coulomb matrix element $V_{c\beta,\varepsilon,k,l}$–this is described in Sec. III–and the matrix elements $\langle\Psi_f^{(N-4)}|a_l a_k|\Psi_i^{(N-2)}\rangle$, where $|\Psi_i^{(N-2)}\rangle$ is a one-determinantal state and where $|\Psi_f^{(N-4)}\rangle$ is allowed to be a general correlated function. In case $|\Psi_f^{(N-4)}\rangle$ is assumed to be also a SCF state, the matrix element $\langle\Psi_f^{(N-4)}|a_l a_k|\Psi_i^{(N-2)}\rangle$ can be expressed by the overlap matrix of the two different orbital sets of the initial and final states, respectively. This is worked out in detail in the Appendix, where the spin-free working equations are derived.

III. CALCULATION OF THE CONTINUUM ORBITAL

As already discussed in the Introduction we have chosen the static-exchange potential [4] (or its generalization to multiconfigurational states) as the interaction potential between the Auger electron and the final dicationic ion. The neglect of the polarization-correlation potential terms is justified by the high kinetic energy of the Auger electron. Moreover, the inclusion of these potential terms would lead to an unbalanced treatment. A balanced treatment including polarization and correlation potential terms would require one to replace the one-channel ansatz (2.5) by a multichannel one [23,24].

We found it convenient to replace the exact exchange by a free-electron-gas model potential [4,14]. As shown in Sec. IV this replacement is justified. Note that the adopted interaction potential is a *local* potential.

A one-particle continuum wave is not entirely specified by its energy ε; two additional quantum numbers are necessary. A particular useful choice is provided by the angular momentum quantum numbers. Hence $\psi_{\varepsilon,l,m}^-$ is a well-defined unique scattering state and we consider the symbol ψ_ε^-, which appeared in the preceding section, as a shorthand notation for $\psi_{\varepsilon,l,m}^-$. (We remind the reader that the minus sign indicates incoming boundary conditions [25], which are required for the computation of the Auger or the photoionization process [26] rather than the more familiar outgoing ones.)

It may be illustrative to unitarily transform the state $\psi_{\varepsilon,lm}^-$ to a Cartesian momentum representation

$$\psi_{\mathbf{k}}^-(\mathbf{r})=k^{-1/2}\sum_{l,m}\psi_{\varepsilon,l,m}^-(\mathbf{r})Y_l^m(\hat{\mathbf{k}})^*\ . \quad (3.1)$$

Here Y_l^m denotes the spherical harmonic function, $\varepsilon = k^2/2$, and $\hat{\mathbf{k}}$ denotes a unit vector pointing into the direction of $\mathbf{k}$, which, in our case, is the direction of the Auger electron. The two equivalent sets of functions satisfy the normalization conditions

$$\langle \psi^-_{\varepsilon,l,m} | \psi^-_{\varepsilon',l',m'} \rangle = \delta(\varepsilon - \varepsilon')\delta_{l,l'}\delta_{m,m'} \tag{3.2}$$

and

$$\langle \psi^-_{\mathbf{k}} | \psi^-_{\mathbf{k}'} \rangle = \delta(\mathbf{k} - \mathbf{k}') , \tag{3.3}$$

respectively. We will make no further use of the set $\{\psi^-_{\mathbf{k}}\}$.

The symmetry properties of the molecule are reflected in the scattered wave, which hence should belong to one of the irreducible representations of the underlying point group. For the general case it may be necessary to linearly combine various $\psi^-_{\varepsilon,l,m}$ of the same energy ε in order to arrive at a scattered wave of proper symmetry. For a linear molecule the situation is particularly simple. All states with $m=0$ are σ states, with $m=\pm 1$ being π states, etc. If there is an inversion center then even l's will give rise to gerade states and odd l's to ungerade states.

We now turn to the computation of the scattered states $\psi^-_{\varepsilon,l,m}$ and write them in a single-center expansion:

$$\psi^-_{\varepsilon,l,m}(\mathbf{r}) = \left[\frac{2}{\pi k}\right]^{1/2} \frac{i^l}{r} e^{-i\sigma_l} \sum_{l',m'} \Phi_{l',m',l,m}(r) Y_{l'}^{m'}(\hat{\mathbf{r}}) . \tag{3.4}$$

where σ_l denotes the Coulomb phase shift [28]. Inserting this ansatz into the Schrödinger equation yields the well-known close-coupling equations [4,25] which are a set of ordinary differential equations for the matrix of solutions $\mathbf{\Phi}$. For a linear molecule this set of coupled differential equations simplifies substantially, because it becomes diagonal in the magnetic quantum number m. A separate calculation for each value of m can be performed. Since the equations are independent of the sign of m, only positive m need be considered. For the sake of notational simplicity we shall drop the index m from all the equations to follow.

The numerical method used by us to solve the close-coupling equations is described in Ref. [27]. The main difference from that previous work on electron scattering lies in the different type of boundary conditions which are now to be satisfied. The solution matrix $\mathbf{\Phi}$ assumes the usual boundary conditions at small r

$$\Phi_{l,l'}(r) \underset{r\to 0}{\to} 0 \tag{3.5}$$

but for large r it is now required to behave like

$$\Phi_{l,l'}(r) \underset{r\to\infty}{\to} \frac{i}{2}\{-[G_l(kr)+iF_l(kr)]\delta_{l,l'} + [G_l(kr)-iF_l(kr)]S^*_{l,l'}\} . \tag{3.6}$$

Here $F_l(kr)$ and $G_l(kr)$ denote the regular and irregular Coulomb waves [28] and $S_{l,l'}$ denote the matrix elements of the $\mathbf{S}$ matrix [25]. In order to compute a solution matrix $\mathbf{\Phi}$ that satisfies these boundary conditions one solves the set of differential equations as an initial-value problem with the initial condition (3.5) and arbitrarily chosen initial derivatives. The thus obtained regular solution matrix $\tilde{\mathbf{\Phi}}$ is finally transformed to obey the correct boundary condition (3.6). To this end we introduce the Wronskian

$$W_{l,l'} = [G_l(kr)-iF_l(kr)]\frac{d}{dr}\tilde{\Phi}_{l,l'}(r) - \frac{d}{dr}[G_l(kr)-iF_l(kr)]\tilde{\Phi}_{l,l'}(r) \tag{3.7}$$

evaluated at the point $r=r_{\text{end}}$, which is the point where the integration stops. The value of r_{end} has to be chosen such that for $r \geq r_{\text{end}}$ the interaction potential is similar to a pure Coulomb potential. Adopting a matrix notation it can be shown [25] that the solution matrix subject to the correct boundary condition (3.6) is given by

$$\mathbf{\Phi}(r) = k\tilde{\mathbf{\Phi}}(r)\cdot\mathbf{W}^{-1} . \tag{3.8}$$

To evaluate $W_{l,l'}$ a knowledge of the Coulomb wave functions F_l and G_l and their derivatives is required. However, it is sufficient to know these functions only at $r=r_{\text{end}}$. At this point kr is a large number and we hence could use an asymptotic expansion [28] to evaluate the Coulomb wave functions.

To determine the Auger rate we have to compute Coulomb matrix elements of the scattered wave. This is done in the following way. We first introduce the functions

$$\chi_{i,j,k}(\mathbf{r}) = \int d\mathbf{r}' \varphi_i(\mathbf{r}')\varphi_j(\mathbf{r})|\mathbf{r}-\mathbf{r}'|^{-1}\varphi_k(\mathbf{r}')^* \tag{3.9}$$

and then express the Coulomb elements by

$$V_{i,j,k,\varepsilon} = \langle \chi_{i,j,k} | \psi^-_{\varepsilon} \rangle . \tag{3.10}$$

The functions $\chi_{i,j,k}$ are computed by introducing a single-center expansion of the SCF orbitals and performing the r integration numerically. The overlap integrals (3.10) are computed simultaneously with the propagation of the wave function. Details are given in Ref. [27].

As mentioned above, the ε appearing in Eq. (3.10) is a shorthand notation for the set (ε,l,m). The Coulomb integrals that involve the scattered wave should carry the angular momentum quantum numbers l and m, in addition. The same is true for the Auger amplitudes [see Eqs. (2.14) and (A14)–(A16)]. For each final dicationic state we hence do not obtain a single Auger amplitude $A \equiv A_{f,i}$ but a family of amplitudes $\{A_{l,m}\}$. These amplitudes can be combined to yield an angle-dependent amplitude

$$A(\mathbf{\Omega}) = \sum_{l,m} A_{l,m} Y_l^m(\mathbf{\Omega}) , \tag{3.11}$$

where $\mathbf{\Omega} \equiv \hat{\mathbf{k}}$ denotes the direction in which the Auger electron is ejected. The differential Auger rate (for a molecule with fixed orientation) is given by

$$\frac{d\sigma}{d\mathbf{\Omega}} = 2\pi |A(\mathbf{\Omega})|^2 , \tag{3.12}$$

and integration over all angles yields the total rate for

production of the dicationic state under consideration

$$\Gamma_{f,i} \equiv \sigma = 2\pi \sum_{l,m} |A_{l,m}|^2. \tag{3.13}$$

IV. AUGER SPECTRUM OF HF

We have calculated the Auger spectrum of hydrogen fluoride in order to test and illustrate the procedure outlined above. The particular example was chosen because there exist experimental data [29] as well as theoretical calculations [13] on the Auger spectrum of HF.

Since the present calculation is the first of its kind we have chosen to treat not only the initial state but also the various final states on the SCF level. Albeit that we are thus neglecting correlation we do describe the relaxation of the orbitals of the initial state and each final state. The consideration of the initial-state relaxation is of particular importance when computing Auger rates [30]. Adopting a Gaussian basis set consisting of $5s/2p$ uncontracted functions centered at the H nucleus and $20s/11p$ $[10s/6p]$ functions centered at the F nucleus we have performed these SCF calculations in two different ways. In the first we have used the conventional restricted Hartree-Fock procedure [31]. In our second approach we define a model closed-shell Fock matrix by

$$F_{i,k} = T_{i,k} + \sum_j n_j (V_{i,j,k,j} - \tfrac{1}{2} V_{i,j,j,k}) \,. \tag{4.1}$$

Here the indices i, j, and k refer to spatial orbitals rather than to spin orbitals. The Symbol n_j stands for the number of electrons in the jth spatial orbital; i.e., $n_j = 0, 1$, or 2. (To ensure the correct spatial symmetry in case of degenerate orbitals, fractional occupation numbers n_j may have to be used.) This method is called the spin-averaged Hartree Fock (SAHF) method because Eq. (4.1) can be obtained from the UHF equations by assuming that the orbitals are independent of the spin. Note that the Fock matrix (4.1) does not depend on the spin of the electronic state to be computed. One obtains the same Fock matrix, for e.g., computing the $^1\Sigma^+(2\sigma^{-1}, 3\sigma^{-1})$ or the $^3\Sigma^+(2\sigma^{-1}, 3\sigma^{-1})$ state (these symbols indicate that the particular state is—when compared to the neutral ground state–characterized by a missing electron in the 2σ orbital and in the 3σ orbital). Equation (4.1) is considered as an orbital generator where the orbitals are found by diagonalizing **F**. The SAHF energies are defined as the expectation values of the Hamiltonian with respect to the SAHF determinant (or linear combination of determinants, when a linear combination is required to satisfy the spin symmetry). The Fock operator (4.1) is, of course, not new; it is often referred to as the *half-electron* Fock operator [32]. For core-ionized states it is better known as the *transition-state* Fock operator [33]. The SAHF calculations are simpler than the RHF ones, because the convergence of the SAHF procedure is better. Furthermore, there are fewer calculations because there is only one orbital set for both the singlet and the triplet states. The use of the SAHF procedure hardly affects the quality of the energy and Auger rates. If anything, we find the rates to be *improved* (see below). We recommend the use of the SAHF rather than the RHF method; in particular, in case of a larger system.

In Table I we show our RHF and SAHF energies in comparison to the RHF energies obtained by Faegri and Kelly [13]. Surprisingly the SAHF energies are *lower* than the RHF energies for those singlet states that have an electron missing in the 2σ orbital. This is because for dicationic states with an inner-valence vacancy the stationary point of the RHF energy functional is a saddle point rather than a local minimum. Enforcing the energy functional to leave the saddle point it will converge to a lower-lying state. We also show in Table I the energy differences between the initial and final states, i.e., the ΔSCF Auger energies and compare them with the experimental data of Shaw and Thomas [29]. The missing correlation in the ΔSCF calculations makes the span of the computed Auger energies too large by about 10%.

One aspect of the present paper is to investigate the

TABLE I. Total energies (in atomic units) and Auger transition energies (in eV). RHF and SAHF stands for the present results obtained with RHF and SAHF orbitals, respectively. FK stands for the RHF results of Faegri and Kelly [13] and Expt. denotes the experimental results of Shaw and Thomas [29]. The internuclear distance in our calculations is $R = 1.7329$ a.u.

State	Total energies (a.u.)			Auger transition energies (eV)			
	RHF	SAHF	FK	RHF	SAHF	FK	Expt.
$^3\Sigma^-(1\pi^{-1}, 1\pi^{-1})$	−98.4128	−98.3933	−98.4140	648.53	648.19	648.31	
$^1\Delta(1\pi^{-2})$	−98.3045	−98.2928	−98.3056	645.58	645.46	645.36	644.28
$^3\Pi(3\sigma^{-1}, 1\pi^{-1})$	−98.2942	−98.2773	−98.2952	645.30	645.03	645.08	
$^1\Sigma^+(1\pi^{-1}, 1\pi^{-1})$	−98.1983	−98.1923	−98.1994	642.69	642.72	642.27	642.35[a]
$^1\Pi(3\sigma^{-1}, \pi^{-1})$	−98.1801	−98.1719	−98.1805	642.19	642.17	641.96	642.35[a]
$^1\Sigma(3\sigma^{-2})$	−97.9986	−97.9986	−98.0005	637.25	637.45	637.06	636.92
$^3\Pi(2\sigma^{-1}, 1\pi^{-1})$	−97.5307	−97.5187	−97.5318	624.52	624.39	624.30	625.1[a]
$^3\Sigma^+(2\sigma^{-1}, 3\sigma^{-1})$	−97.4130	−97.3944	−97.4141	621.32	621.01	621.10	625.1[a]
$^1\Pi(2\sigma^{-1}, 1\pi^{-1})$	−97.1648	−97.1667	−97.1662	614.57	614.82	614.36	616.2
$^1\Sigma^+(2\sigma^{-1}, 3\sigma^{-1})$	−97.0470	−97.0473	−97.0810	611.36	611.45	612.04	614.1
$^1\Sigma^+(2\sigma^{-2})$	−96.3274	−96.3274	−96.3270	591.78	591.98	591.52	595.6
$^2\Sigma^+(1\sigma^{-1})$	−74.5786	−74.5714	−74.5878				

[a]Assigned to two lines, since experimentally unresolved.

dependence of the computed Auger rates on the approximation for the wave function. Table II shows the Auger rates computed by assuming the continuum orbital to be a plane wave, a Coulomb wave, or a molecular scattered wave. For each state there are two entries in the table. The lower (upper) entry refers to a calculation where the continuum orbital is (not) orthogonalized to the occupied orbitals of the initial state [i.e., $V_{c\beta,\epsilon_1,k,l}$ ($V_{c\beta,\epsilon,k,l}$) is used in Eqs. (2.14) and (A14)–(A16)]. The calculation using plane or Coulomb waves yields reasonable results for *singlet* states with vacancies in the outer valence orbitals. The rates for the corresponding *triplet* states are always severely too large. For the final dicationic states that contain a 2σ hole the rates are unequivocally very unreliable. Generally, the rates computed using plane or Coulomb waves vary strongly according to whether or not these waves are orthogonalized to the occupied orbitals of the initial $^2\Sigma(1\sigma^{-1})$ core-hole state. This fact again emphasizes the poor quality of plane or Coulomb waves for the computation of Auger rates. In high-quality computations the final continuum state should *a priori* be nearly orthogonal to the initial state.

We now turn to the Auger rates computed with molecular continuum waves. To investigate the dependence of the computed rates on the potential used to determine the continuum orbital we have listed in Table II the results obtained with three different potentials. The third and the fourth columns of Table II show the results obtained with the static potential and the static-exchange potential of the $^1\Sigma^+(3\sigma^{-2})$ final state. The inclusion of the exchange interaction changes the rates by typically 5% [12% for the $^3\Pi(3\sigma^{-1},1\pi^{-1})$ state]. Hence the contribution of the exchange potential is not negligible, but it is small and the use of a local model exchange seems to be appropriate.

Turning to discuss again the effect of the orthogonalization we remark that the quality of the continuum orbital is quite directly indicated by the difference caused upon orthogonalization (i.e., the difference between upper and lower entries). This difference monotonically decreases when the quality of the interaction potential (no potential, static potential, static-exchange potential) is improved.

To be consistent one should compute the continuum wave with respect to that static-exchange potential that is defined by the charge distribution of the particular final dicationic state under discussion. Thus one should compute as many static-exchange potentials as there are final states. Luckily it turns out that a single potential is sufficient to compute the molecular continuum waves for all final states. The last two columns of Table II show Auger rates evaluated with scattered waves that are computed by assuming two different potentials; namely, the static-exchange potential of the $^1\Sigma^+(3\sigma^{-2})$ and

TABLE II. Calculated Auger transition rates of HF (in 10^{-3} a.u.). Test of different potentials. The rates are computed using for the continuum orbital a plane wave, a Coulomb wave, or a scattered molecular wave. The latter wave is calculated on the static or the static-exchange level. Results are shown for the potentials obtained from RHF calculations on the $^1\Sigma^+(3\sigma^{-2})$ and $^1\Sigma^+(2\sigma^{-2})$ states. For each final state there are two entries. The lower (upper) entry indicates that the continuum orbital is (not) orthogonalized to the occupied orbitals of the initial state.

			$^1\Sigma^+(3\sigma^{-2})$		$^1\Sigma^+(2\sigma^{-2})$
State	Plane	Coulomb	Static	Static exchange	Static exchange
$^3\Sigma^-(1\pi^{-1},1\pi^{-1})$	0.0	0.0	0.0	0.0	0.0
$^1\Delta(1\pi^{-2})$	2.3305	2.0878	1.8702	1.8461	1.8335
	2.3305	2.0878	1.8702	1.8461	1.8335
$^3\Pi(3\sigma^{-1},1\pi^{-1})$	0.2848	0.1820	0.0487	0.0436	0.0434
	0.1598	0.1204	0.0471	0.0433	0.0430
$^1\Sigma^+(1\pi^{-1},1\pi^{-1})$	0.5755	0.3531	0.5583	0.5459	0.5419
	0.3934	0.5038	0.5778	0.5573	0.5537
$^1\Pi(3\sigma^{-1},1\pi^{-1})$	1.9356	1.7444	1.5719	1.5584	1.5590
	1.9385	1.7471	1.5720	1.5585	1.5588
$^1\Sigma^+(3\sigma^{-2})$	0.6197	0.4923	0.5093	0.5077	0.5119
	0.5419	0.5410	0.5191	0.5135	0.5162
$^3\Pi(2\sigma^{-1},1\pi^{-1})$	3.6060	2.3220	0.6398	0.5744	0.5733
	1.9728	1.5136	0.6187	0.5697	0.5665
$^3\Sigma^+(2\sigma^{-1},3\sigma^{-1})$	1.6078	1.0307	0.2775	0.2507	0.2508
	0.9691	0.7198	0.2679	0.2473	0.2481
$^1\Pi(2\sigma^{-1},1\pi^{-1})$	0.2427	0.5734	1.2724	1.3017	1.2996
	0.3167	0.6403	1.2767	1.3027	1.3013
$^1\Sigma^+(2\sigma^{-1},3\sigma^{-1})$	0.1027	0.2579	0.5492	0.5605	0.5611
	0.1218	0.2537	0.5469	0.5587	0.5603
$^1\Sigma^+(2\sigma^{-2})$	0.6326	1.1146	1.0064	0.9568	0.9548
	0.2419	0.0327	0.8583	0.8692	0.8668

$^1\Sigma^+(2\sigma^{-2})$ states, respectively. The differences are always below 1%, and we have found similar results by using static-exchange potentials created by the charge distribution of other dicationic states.

Closing the discussion of Table II we conclude that the total neglect of the interaction potential (i.e., using plane waves) or the use of a Coulomb wave are not justified for computing Auger rates. On the other hand, the dependence of the rate on the interaction potential is not so strong that small changes in the potential matter. This insensitivity originates partly from the high energy of the Auger electron. More important seems to be the fact that the Auger process probes only that part of the scattered wave that is spacewise close to the core-hole orbital of the initial state. The use of the correct potential will become important when the angular distribution of the Auger electron is investigated. The angular distribution is determined by the asymptotic part of the scattered wave, which, in turn, is quite sensitive to the potential.

Having found that it is sufficient to use one single potential to compute the scattered waves for all final states, we have used the static-exchange potential of the $^1\Sigma^+(3\sigma^{-2})$ state in the calculations to be discussed below. In Table III we investigate the influence of some approximations on the formulas of the Auger rates. The first approximation ignores the influence of the overlap matrix **S** (not to be confused with the scattering **S** matrix) between the sets of orbitals of the initial and final states, i.e., we replace **S** by the unit matrix [see Eqs. (A12)–(A16)]. The second (already mentioned) approximation ignores the orthogonalization of the continuum wave. The thus obtained Auger rates are given in Table III, together with the results of Faegri and Kelly [13]. The dependence of the Auger rates on both the overlap matrix and the orthogonalization is rather small except for the rates of those states that contain a 2σ hole. We presume that the small influence of the overlap matrix is peculiar to the HF molecule. The Auger rates of molecules with a more covalent rather than ionic bond might show a more pronounced dependence on the neglect of the overlap matrix. Indeed, Jennison [30] has found the inclusion of the overlap matrix to be important when investigating the Auger spectrum of ethane.

The rather small dependence of the Auger rates on the orthogonalization of the continuum orbital shows that the scattered wave is almost orthogonal to the occupied orbitals of the *initial* state. This is partly due to the large energy separation between the occupied orbitals and the continuum wave. We recall that a rigorous formulation for the continuum wave requires $a_\varepsilon|\Psi_f^{(N-2)}\rangle=0$ but there are no physical reasons why $a_\varepsilon|\Psi_i^{(N-1)}\rangle=0$ should hold rigorously.

Faegri and Kelly have ignored the overlap matrix in their calculations and they have approximated the molecular continuum wave by an atomic one. For the HF molecule these approximation are not severe, and one finds a

TABLE III. Calculated Auger transition rates of HF (in 10^{-3} atomic units). Test of different evaluation formulas. The static-exchange potential of the $^1\Sigma^+(3\sigma^{-2})$ state is used to compute the molecular continuum wave. Shown are the results obtained with the RHF and SAHF approaches using the full overlap between the orbitals of the initial and final states and also neglecting the overlap (indicated by no overlap). For each final state there are two entries. The lower (upper) entry indicates that he continuum orbital is (not) orthogonalized to the occupied orbitals of the initial state. The results of Faegri and Kelly [13] are shown for comparison.

State	FK	RHF no overlap	RHF	SAHF no overlap	SAHF
$^3\Sigma^-(1\pi^{-1},1\pi^{-1})$	0.0	0.0	0.0	0.0	0.0
$^1\Delta(1\pi^{-2})$	1.986	1.8607	1.8461	1.9019	1.8739
		1.8607	1.8461	1.9019	1.8739
$^3\Pi(3\sigma^{-1},1\pi^{-1})$	0.021	0.0274	0.0436	0.0215	0.0196
		0.0272	0.0433	0.0213	0.0194
$^1\Sigma^+(1\pi^{-1},1\pi^{-1})$	0.594	0.5504	0.5459	0.5707	0.5623
		0.5619	0.5573	0.5717	0.5633
$^1\Pi(3\sigma^{-1},1\pi^{-1})$	1.692	1.5757	1.5584	1.5968	1.5737
		1.5758	1.5585	1.5969	1.5738
$^1\Sigma^+(3\sigma^{-2})$	0.564	0.5128	0.5077	0.5187	0.5143
		0.5186	0.5135	0.5213	0.5169
$^3\Pi(2\sigma^{-1},1\pi^{-1})$	0.574	0.5927	0.5744	0.4548	0.4362
		0.5879	0.5697	0.4509	0.4325
$^3\Sigma^+(2\sigma^{-1},3\sigma^{-1})$	0.302	0.2540	0.2507	0.1957	0.1920
		0.2506	0.2473	0.1930	0.1893
$^1\Pi(2\sigma^{-1},1\pi^{-1})$	1.288	1.3123	1.3017	1.0689	1.0557
		1.3133	1.3027	1.0702	1.0569
$^1\Sigma^+(2\sigma^{-1},3\sigma^{-1})$	0.642	0.6559	0.5605	0.5321	0.5220
		0.6450	0.5587	0.5266	0.5166
$^1\Sigma(2\sigma^{-2})$	0.983	1.0748	0.9568	0.8008	0.7121
		0.9734	0.8692	0.7519	0.6703

reasonable agreement between the Auger rates computed by Faegri and Kelly and our RHF results (see Table III).

All the Auger rates discussed so far have been evaluated by using the RHF orbitals. The last two columns of Table III depict the Auger rates computed with SAHF orbitals for both the initial and the final states. We have found the rates to be very insensitive to the choice of the specific Hartree-Fock procedure applied to the final states; only the Hartree-Fock procedure of the initial state matters. There is a noticeable effect only on the rates of those final states that contain a 2σ hole; these rates are decreased when using the SAHF procedure. This is mainly due to the fact that the SAHF 1σ core orbital of the initial state is slightly more compact than the RHF one.

All the data on the rates reported so far were obtained by employing the first term of Eq. (2.14) only. As already discussed in Sec. II the third term of Eq. (2.14) yields a contribution that is negligible in the case of the HF molecule, and we presume this to be true for most other molecules as well. The second term of Eq. (2.14) vanishes identically when using the RHF orbitals. For SAHF orbitals, however, this term does not vanish but reduces to

$$-\tfrac{1}{2}\sum_{j,k}^{\text{occ}} V_{c\beta,c\alpha,j,c\alpha}\langle \psi_\varepsilon^- | \varphi_k \rangle \langle \Psi_f^{(N-4)} | a_j a_k | \Psi_i^{(N-2)} \rangle \ . \quad (4.2)$$

This term is usually small because the overlaps $\langle \psi_\varepsilon^- | \varphi_k \rangle$ (k occupied) are small. However, the overlaps are not small if a scattered wave of low quality (e.g., a plane wave) is used. In this case (4.2) leads to a spurious contribution and the second term of Eq. (2.14) *should* be discarded.

Using the SAHF orbitals and the molecular scattered wave we have found that the inclusion of (4.2) always increases the rates; however, this effect is worth mentioning only for those final dicationic states that contain a 2σ hole. By far the largest effect is found for the $^1\Sigma^+(2\sigma^{-2})$ state. Here we computed a rate of 0.7574×10^{-3} a.u. when including the term (4.2). This rate lies right in between the rates computed with the RHF orbitals (0.8692×10^{-3} a.u.) and the rates computed with the SAHF orbitals, while ignoring (4.2) (0.6703×10^{-3} a.u.) (see Table III).

The use of the SAHF orbitals yields the best results for the rates when compared to experiment. In Fig. 1 we compare our final results (last column of Table III) with the experimental data of Shaw and Thomas [29]. All features of the experimental spectrum are nicely reproduced by the calculation. Only the small peak at ~630 eV, which is visible in the experimental spectrum, does not appear in our calculation. This peak can be attributed to shake-off satellites. We computed the ΔSCF energies of the $^1\Pi(1\sigma^{-1},1\pi^{-1})\rightarrow{}^2\Pi(1\pi^{-3})$ and the $^3\Pi(1\sigma^{-1},1\pi^{-1})\rightarrow{}^2\Pi(1\pi^{-3})$ transitions to be 627.9 and 631.3 eV, respectively. This nicely explains the small discrepancy, even though we have not computed the Auger rates of these transitions.

In Fig. 1 and all other figures we have convoluted the computed stick spectrum with Gaussians to make the comparison with the experimental data more vivid. The

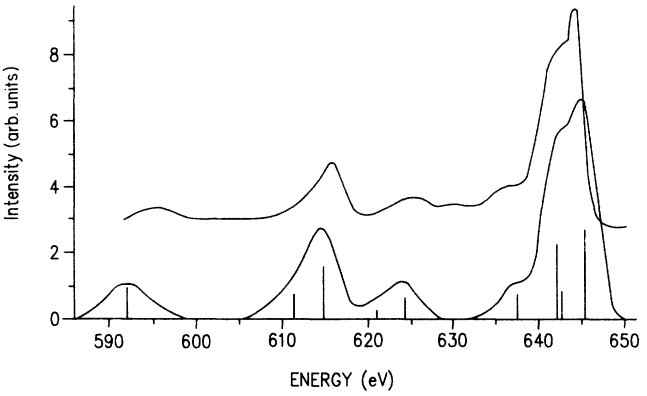

FIG. 1. Comparison of the computed Auger spectrum with experimental data. The computed stick spectrum is convoluted with normalized Gaussians of widths [$^1\Sigma(2\sigma^{-2})$, 6.0; $^1\Sigma(2\sigma^{-1},3\sigma^{-1})$, 5.0; $^3\Sigma(2\sigma^{-1},3\sigma^{-1})$, $^1\Pi(2\sigma^{-1},1\pi^{-1})$, and $^3\Pi(2\sigma^{-1},1\pi^{-1})$, 4.0; $^1\Sigma(3\sigma^{-2})$, 4.5; $^1\Pi(3\sigma^{-1},1\pi^{-1})$ and $^1\Sigma(1\pi^{-1},1\pi^{-1})$, 3.8; $^3\Pi(3\sigma^{-1},1\pi^{-1})$ and $^1\Delta(1\pi^{-2})$, 3.1; in eV, full width at half maximum] to be more easily compared to the experimental data. The energies and rates employed for the theoretical curve are those obtained by using the SAHF orbitals (see Tables I and III, intensities in arbitrary units).

other way around, namely, the deconvolution of the Auger rates from a spectrum consisting of overlapping peaks, is a very unstable procedure and we thus do not compare those numbers. (The experimental determination of the Auger energies, as given in Table I, may also suffer from this instability.)

In Fig. 2 we compare the results of Faegri and Kelly with our results obtained with both the RHF and the SAHF orbitals. This figure also illustrates the difference in the rates caused by adopting different sets of orbitals.

We finally want to demonstrate the already discussed failure of the use of plane or Coulomb waves. Figure 3 compares our final results with the rates computed by using orthogonalized or nonorthogonalized plane or Coulomb waves. The high-energy peak of the Auger

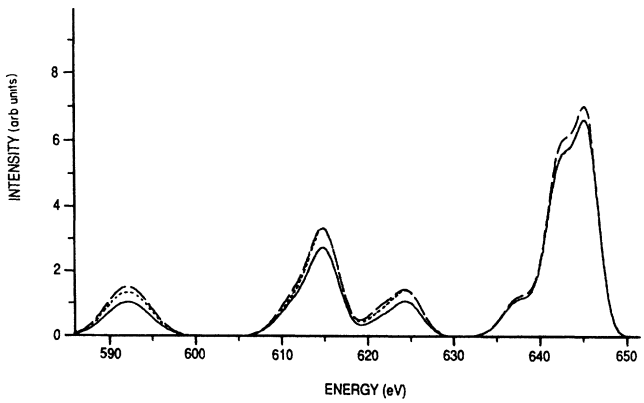

FIG. 2. Comparison of the Auger spectrum obtained by using SAHF orbitals (solid line), RHF orbitals (dotted line) with the data computed by Faegri and Kelly (dashed line). The Gaussians used for the convolution are the same as in Fig. 1.

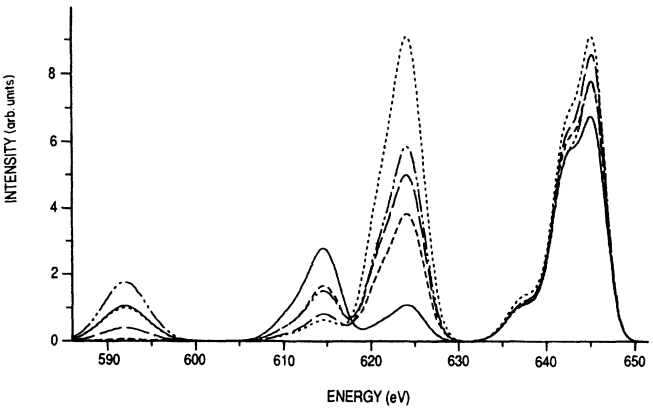

FIG. 3. Comparison of the Auger spectra obtained by using plane or Coulomb waves with the one obtained by using the wave scattered by the static-exchange potential (——). Plane wave (· · ·), plane wave orthogonalized (— — —), Coulomb wave (—··—··), and Coulomb wave orthogonalized (- - -).

spectrum (corresponding to the ground and the first three excited dicationic states) is fairly well reproduced by these approximations but all the rest of the Auger spectrum is in error.

V. CONCLUDING REMARKS

In this paper we proposed a method to calculate Auger rates. The approach is based on three assumptions, namely, the following.

(i) The Auger effect can be considered as a two-step process (ionization and decay), and a nonrelativistic first-order treatment is sufficient (Wentzel's ansatz).

(ii) The core-valence separation is valid when evaluating the wave functions in the expressions for the rates.

(iii) The ejected Auger electron does not correlate with the other electrons of the residual dication.

We emphasize again that the first assumption implies the validity of the second one (see Sec. II).

We have paid particular attention to the evaluation of the continuum wave function of the ejected Auger electron. In the present work we have adopted the molecular static-exchange potential to compute this scattered wave. The wave function of the Auger electron has thus the correct spatial symmetry, and computation of the angular distribution of the Auger electron of aligned molecules is possible.

For the present calculation on the Auger spectrum of hydrogen fluoride we have further approximated the initial core-ionized state and the final dicationic states by SCF determinants. This approximation is not necessary in the present formalism, and multiconfigurational wave functions can be used as well. Hence the correlation in the initial core-hole state and—more important—in the final dicationic state can be accounted for in a rather straightforward way. Since we are dealing with numerical wave functions for the Auger electron, the treatment of the final-state-channel coupling [23,24] is more involved technically.

When performing the numerical calculation of the Auger spectrum of hydrogen fluoride our emphasis was not only to interpret an experiment, but in particular to investigate the importance of different terms. We have found that the Auger rates change very little when using a single-interaction potential to compute the scattered waves of all final states, rather than using a different static-exchange potential for the computation of the scattered wave of each individual final state.

We further have found that ignoring the overlap matrix between the orbital sets of the initial and final states introduces only small changes into the compound Auger rates. We assume that this weak dependence on the overlap matrix is peculiar to hydrogen fluoride. The dependence on the overlap matrix may be stronger [30] for molecules where the bond has a more pronounced covalent character.

Finally, it has turned out that the orthogonalization of the scattered wave with respect to the occupied orbitals of the *initial* state changes the Auger rates only slightly. Only states with inner-valence holes [in particular the $^1\Sigma^+(2\sigma^{-2})$ state] show a noticeable effect. This, we presume, might be true for other molecules as well. On the other hand, for scattered waves of poor quality—like plane or Coulomb waves—the orthogonalization changes the Auger rates substantially; however, not always improving them.

ACKNOWLEDGMENTS

The authors thank F. Tarantelli for discussions. We thank the Deutsche Forschungsgemeinschaft (DFG) for financial support.

APPENDIX: SPIN-FREE WORKING EQUATIONS

In this appendix we specify the final states and derive the spin-free working equations for the Auger rates. An index in Latin letters refers in this appendix to the spatial part of an orbital only. The spin part is denoted by Greek letters, where α stands for spin up and β for spin down. Since the orbitals of the final states are different from those of the initial state, the prior orbitals and their creation operators are denoted by χ and $b^\dagger$ rather than by φ and $a^\dagger$.

In order to satisfy the spin symmetry one cannot always write the final state as a single determinant but must represent it as a sum of several determinants. We found it convenient to define these determinants with respect to

$$|\Phi_0^{(N)}\rangle = \prod_{k=1}^{N} b_{k\alpha}^\dagger b_{k\beta}^\dagger |0\rangle \ ,$$

where $|0\rangle$ is the vacuum and each final state is assumed to have its own set of creation operators.

We now define the final dicationic states of correct spin symmetry and consider the three cases possible for a closed-shell target.

Case a. Singlet, both electrons are removed from the same orbital:

$$|\Psi_f^{(N-2)}\rangle = b_{n\beta} b_{n\alpha} |\Phi_0^{(N)}\rangle \ , \tag{A1}$$

Case b. Singlet, two electrons are removed from different orbitals:

$$|\Psi_f^{(N-2)}\rangle = 2^{-1/2}\{b_{n\alpha} b_{m\beta} - b_{n\beta} b_{m\alpha}\} |\Phi_0^{(N)}\rangle \ . \tag{A2}$$

Case c. Triplet:

$$|\Psi_f^{(N-2)}, M_S = 0\rangle = 2^{-1/2}\{b_{n\alpha} b_{m\beta} + b_{n\beta} b_{m\alpha}\} |\Phi_0^{(N)}\rangle \tag{A3}$$

and

$$|\Psi_f^{(N-2)}, M_S = 1\rangle = b_{n\beta} b_{m\beta} |\Phi_0^{(N)}\rangle \ . \tag{A4}$$

Here M_S denotes the eigenvalue of the spin operator S_Z. We have assumed that the orbitals χ_j satisfy the correct spatial symmetry requirements; e.g., in case of a linear molecule one may have to unitarily transform the degenerate π orbitals, such that the new orbitals are eigenfunctions of the angular momentum operator L_Z. The working equations expressed in the original orbitals may then contain additional terms.

The initial state is a doublet state of spin α [see Eq. (2.6)]. The $(N-1)$ final state (i.e., including the continuum wave) must hence also be a doublet state of spin α. A short calculation shows that the $(N-1)$ final state of correct spin symmetry takes the form

$$|\Psi_f^{(N-1)}\rangle = a_{\varepsilon\alpha}^{\dagger} |\Psi_f^{(N-2)}\rangle \tag{A5}$$

if the final dicationic state is a singlet and

$$|\Psi_f^{(N-1)}\rangle = (\tfrac{2}{3})^{1/2} a_{\varepsilon\beta}^{\dagger} |\Psi_f^{(N-2)}, M_S = 1\rangle + (\tfrac{1}{3})^{1/2} a_{\varepsilon\alpha}^{\dagger} |\Psi_f^{(N-2)}, M_S = 0\rangle \tag{A6}$$

for a final $(N-2)$ triplet state. For a linear molecule the spatial symmetry of the final $(N-1)$ state must be Σ^+. The scattered wave ψ_{ε}^- must hence have σ, π, or δ symmetry when the final dicationic state is of Σ^+, Π, or Δ symmetry, respectively. A Σ^- state is dark.

Our equation for the Auger amplitude [Eq. (2.14) first term] now reads

$$A_{f,i} = \sum_{k,l}^{\text{occ}} V_{c,\varepsilon_\perp,k,l} \langle \Psi_f^{(N-4)} | a_{l\alpha} a_{k\beta} | \Psi_i^{(N-2)} \rangle \tag{A7}$$

when the final state is a singlet and

$$A_{f,i} = \sum_{k,l}^{\text{occ}} V_{c,\varepsilon_\perp,k,l} [(\tfrac{2}{3})^{1/2} \langle \Psi_f^{(N-4)}, M_S = 1 | a_{l\beta} a_{k\beta} | \Psi_i^{(N-2)} \rangle + (\tfrac{1}{3})^{1/2} \langle \Psi_f^{(N-4)}, M_S = 0 | a_{l\alpha} a_{k\beta} | \Psi_i^{(N-2)} \rangle] \tag{A8}$$

when the final dicationic state is a triplet.

In order to proceed we introduce the following matrices:

$$Q_{k,l}^{n,m} = \langle \Phi_0^{(N-2)} | b_{n\beta}^{\dagger} b_{m\alpha}^{\dagger} a_{l\alpha} a_{k\beta} | \Psi_i^{(N-2)} \rangle \tag{A9}$$

and

$$\tilde{Q}_{k,l}^{n,m} = \langle \Phi_0^{(N-2)} | b_{n\beta}^{\dagger} b_{m\beta}^{\dagger} a_{k\beta} a_{l\beta} | \Psi_i^{(N-2)} \rangle \ , \tag{A10}$$

where $|\Phi_0^{(N-2)}\rangle$ denotes a determinant similar to $|\Phi_0^{(N)}\rangle$ but with the two core orbitals removed.

Using the technique of biorthogonalized orbitals, as described in the Appendix of Ref. [7], it is easy to express these matrices in terms of the overlap matrix

$$S_{ij} = \langle \chi_i | \varphi_j \rangle \tag{A11}$$

between the sets of orbitals of the initial and final states. After some algebra one arrives at

$$Q_{k,l}^{n,m} = (\mathbf{S}^{-1})_{k,n} (\mathbf{S}^{-1})_{l,m} [\det(\mathbf{S})]^2 \tag{A12}$$

and

$$\tilde{Q}_{k,l}^{n,m} = Q_{k,l}^{n,m} - Q_{l,k}^{n,m} \ . \tag{A13}$$

Now we can write the Auger amplitude for the three cases introduced above as the following.

Case a (singlet),

$$A_{f,i} = \sum_{k,l}^{\text{occ}} V_{c,\varepsilon_\perp,k,l} Q_{k,l}^{n,n} \ . \tag{A14}$$

Case b (singlet),

$$A_{f,i} = 2^{-1/2} \sum_{k,l}^{\text{occ}} V_{c,\varepsilon_\perp,\{k,l\}} Q_{k,l}^{n,m} \ , \tag{A15}$$

where $V_{i,j\{k,l\}} = V_{i,j,k,l} + V_{i,j,l,k}$.

Case c (triplet),

$$A_{f,i} = (\tfrac{3}{2})^{+1/2} \sum_{k,l}^{\text{occ}} V_{c,\varepsilon_\perp,[k,l]} Q_{k,l}^{n,m} \ , \tag{A16}$$

where $V_{i,j,[k,l]} = V_{i,j,k,l} - V_{i,j,l,k}$. This concludes our deviation. The working equations are (2.15), (3.13), (A12), and (A14)–(A16).

[1] H. Ågren, J. Chem. Phys. **75**, 1267 (1981), and references therein; P.E.M. Siegbahn, Chem. Phys. **66**, 443 (1982).

[2] C.-M. Liegener, J. Chem. Phys. **79**, 2924 (1983); Chem. Phys. **106**, 201 (1984), and references therein.

[3] F. Tarantelli, A. Tarantelli, A. Sgamellotti, J. Schirmer, and L. S. Cederbaum, J. Chem. Phys. **83**, 4683 (1985); F. Tarantelli, A. Sgamellotti, and L. S. Cederbaum, *ibid.* **94**, 523 (1991).

[4] N. F. Lane, Rev. Mod. Phys. **52**, 29 (1981).

[5] R. R. Lucchese, K. Takatsuka, and V. McKoy, Phys. Rep.

131, 147 (1986).
[6] B. I. Schneider and L. A. Collins, Comput. Phys. Rep. **10**, 49 (1989).
[7] J. Schirmer, M. Braunstein, and V. McKoy, Phys. Rev. A **41**, 283 (1990).
[8] R. Colle, S. Simonucci, and T. O. Woodruff, Phys. Rev. A **38**, 694 (1988).
[9] F. O. Ellison, J. Chem. Phys. **61**, 507 (1974).
[10] B. Ritchie, J. Chem. Phys. **60**, 898 (1974).
[11] H. Siegbahn, L. Asplund, and P. Kelfve, Chem. Phys. Lett. **35**, 330 (1975).
[12] D. R. Jennison, Chem. Phys. Lett. **69**, 435 (1980).
[13] K. Faegri, Jr. and H. P. Kelly, Phys. Rev. A **19**, 1649 (1979).
[14] S. Hara, J. Phys. Soc. Jpn. **22**, 710 (1967).
[15] M. Higashi, E. Hiroike, and T. Nakajima, Chem. Phys. **68**, 377 (1982).
[16] F. P. Larkins and J. A. Richards, Aust. J. Phys. **39**, 809 (1986).
[17] R. Colle and S. Simonucci, Phys. Rev. A **39**, 6247 (1989).
[18] V. Carravetta and H. Ågren, Phys. Rev. A **35**, 1022 (1987).
[19] P. W. Langhoff, in *Electron-Molecule and Photon-Molecule Collisions,* edited by T. Rescigno, V. McKoy, and B. Schneider (Plenum, New York, 1979), p. 183.
[20] G. Wentzel, Z. Phys. **43**, 521 (1927).
[21] R. Manne and H. Ågren, Chem. Phys. Lett. **93**, 201 (1985).
[22] A. L. Fetter and J. D. Walecka, *Quantum Theory of Many Particle Systems* (McGraw-Hill, New York, 1971).
[23] G. Howat, T. Aberg, and O. Goscinski, J. Phys. B **11**, 1575 (1978).
[24] R. Colle and S. Simonucci, Phys. Rev. A **42**, 3913 (1990).
[25] J. R. Taylor, *Scattering Theory* (Wiley, New York, 1972).
[26] K. Gottfired, *Quantum Mechanics* (Benjamin, New York, 1966).
[27] H.-D. Meyer, Phys. Rev. A **34**, 1797 (1986).
[28] *Handbook of Mathematical Functions,* edited by M. Abramowitz and I. A. Stegun (Dover, New York, 1964).
[29] R. W. Shaw and T. D. Thomas, Phys. Rev. A **11**, 1491 (1975).
[30] D. R. Jennison, Phys. Rev. A **23**, 1215 (1981).
[31] C.C.J. Roothan, Rev. Mod. Phys. **32**, 179 (1960).
[32] H. C. Longuet-Higgins and J. A. Pople, Proc. Phys. Soc. London Sect. A **68**, 591 (1955).
[33] O. Goscinski, B. T. Pickup, and G. Purvis, Chem. Phys. Lett. **22**, 167 (1973).